Catalysis Today 145 (2009) 76–84

Contents lists available at ScienceDirect

Catalysis Today

journal homepage: www.elsevier.com/locate/cattod

Macronized aligned carbon nanotubes for use as catalyst support and ceramic nanoporous membrane template

Izabela Janowska *, Shabnam Hajiesmaili, Dominique Bégin, Valérie Keller, Nicolas Keller, Marc-Jacques Ledoux, Cuong Pham-Huu

Laboratoire des Matériaux, Surfaces et Procédés pour la Catalyse (LMSPC), European Laboratory for Catalysis and Surface Sciences (ELCASS), CNRS, Louis Pasteur University, 25 rue Becquerel, 67087 Strasbourg, France

ARTICLE INFO

Article history:
Available online 5 August 2008

Keywords:
Aligned carbon nanotube array
Self-supported carbon nanotubes
Catalyst support
Ceramic nanoporous membrane
β-SiC

ABSTRACT

An aligned carbon nanotube carpet was synthesized by catalytic chemical vapor deposition (CCVD) process at 800 °C with a mixture of ferrocene and toluene, using a removable quartz substrate as macroscopic pre-form. The strong anchorage of the aligned nanotube array at the macroscopic host surface allows the nano–macro-composite to be considered as a nano-ordered macroscopic material and self-supported aligned nanotubes could be obtained by substrate removal. The carpet thickness could be accurately controlled from few tenth micrometers to more than few millimeters by tuning the synthesis duration. Such a nano–macro-composite could be used as high contact surface catalyst support with low pressure drop. The aligned nanotube array was efficiently used as removable precursor template in the design of β-SiC ceramic nanoporous membranes.

1. Introduction

Since their discovery in 1991 by Iijima [1], carbon nanotubes have received an increasing scientific interest because of their exceptional physical properties [2–6]. The most promising route to generate carbon nanotubes is the catalytic chemical vapour deposition (CCVD), based on the low temperature decomposition of a gaseous carbon source with or without hydrogen over a catalyst [7–11]. For nanotechnology devices, the development of synthesis methods to form macroscopic and organized carbon nanotubes is required. Indeed, the ultimate goal of carbon nanotube research is driven by the ability to design functional macroscopic structures that can fully integrate the single nanotube properties. Several works have been published during the last decades dealing with the synthesis of carbon nanofibers anchored at the surface of a macroscopic host structure [12–17]. These composites display a huge advantage compared to traditional catalyst supports, namely a high external surface area due to the presence of nanomaterials at the topmost surface combined to an easy handling owing to the macroscopic shaping. The macroscopic shaping also reduces the problem of nanomaterial dispersing or loss during handling and allows the direct use of nanoscale materials within conventional catalytic reactors by drastically reducing the pressure drop compared to bulk nanoscopic materials and avoiding restrictive moving-bed phenomena.

Parallely, aligned multi-walled carbon nanotubes produced by CCVD methods have been received an increasing interest during the last decade [18–21]. Pioneering works have been published by both Maruyama's group [22,23], and Resasco's group [24] on the vertical growth of aligned single-walled carbon nanotubes on a macroscopic flat substrate by direct decomposition of gaseous hydrocarbons over a Co–Mo catalyst. Janowska et al. have recently reported the growth of aligned carbon nanotubes on different quartz substrates for direct use as catalyst support in liquid-phase hydrogenation [25]. From these results, one should expect that the scaling up and the macronization of carbon nanomaterials could have been deeply investigated, resulting in well-controlled structures, for opening a new era in term of industrial applications. However, to date, the use of aligned carbon nanotube structures remained mainly focused in fields such as electronic, filtration or conductive polymer fabrication [26–29], while the catalysis field remains very scarcely investigated [25].

Combining a macroscopic shaping and the high external surface area exposed by the aligned carbon nanotube material (due to the nanoscopic size of the tube) could allow the use of these materials in the field of structured reactors, by favoring both heat and mass transfers together with the easy recovery of both catalyst and products at the end of the test. It is expected that specific properties could be observed, especially in the heterogeneous catalysis field, compared to those usually shown by powder, grain

* Corresponding author. Tel.: +33 3 90 24 26 75; fax: +33 3 90 24 26 74.
E-mail address: Izabela.Janowska@ecpm.u-strasbg.fr (I. Janowska).

0920-5861/$ – see front matter © 2008 Elsevier B.V. All rights reserved.
doi:10.1016/j.cattod.2008.06.020

or extrudate traditional catalysts. The main advantage of using these materials relies on their high external surface area which could strongly increase the contact surface between the reactants and the active sites. Previous results have shown that active phase located inside the carbon nanotube cavity exhibits an extremely high activity compared to that observed on traditional grain size catalysts [30–32]. Since future progresses in catalysis closely depend partly on the development of new catalytic materials with smart characteristics, technology is therefore constantly pushing towards smaller materials with improved properties, *i.e.* activity and especially selectivity for minimizing by-products and the cost-incentive waste disposal. High selectivity also allows the post-reaction separation steps to be reduced for significantly decreasing the process costs.

Another field that can benefit from the use of nanomaterial devices, concerned the separation technology [33–35] and among such processes, the filtration area especially. Filtration of airborne particulate matter is essential in many instances, including air purifiers, respiratory protection device and clean rooms. Within the filtration area, the detoxificating filtration of contaminated or polluted water could also be improved by using nanomaterials. Nanofilters should have controlled geometric shapes, with both tailorable density and size for meeting the requirements of high-technology applications. In summary, high efficiency filtration device should be designed with appropriate large-scale macro-nized structures incorporating nanoscale tailored sub-units. Finally, filters need to be robust and should withstand repeated regeneration steps for reducing the waste disposal costs, one of the most environmental concern today.

Here we report on the synthesis of macroscopic devices with different sizes and shapes containing well-aligned carbon nanotubes obtained by the CCVD method carried out using a quartz substrate as macroscopic host structure. SiC ceramic nanoporous membrane was also prepared, using the aligned carbon nanotube carpet as precursor replica template, to illustrate a possible application of the nano–macro-composites. Indeed, typical filters are an assembly of 10 μm mean diameter fibers, this diameter being a parameter that strongly affects the efficiency of usual filter devices. It is expected that filter materials with smaller diameter nanoscale 1D-structures, such as nanotubes or nanochannels, should display unique properties owing to their small dimensions.

2. Experimental

2.1. Synthesis of the aligned carbon nanotube array coating

The aligned carbon nanotube pattern was synthesized via the CCVD method, using a mixture of $Fe(C_5H_5)_2$ ferrocene – $FeCp_2$– acting as catalyst, and toluene acting as carbon source within an argon stream. The ferrocene concentration in the toluene solution was 20 g L^{-1}. The liquid $FeCp_2$–C_7H_8 mixture was feed into the reaction zone through a high speed nozzle and further vaporized leading to the formation of a mist which was carried out into the reaction zone by a 1.5 L min^{-1} argon flow. The synthesis was carried out at 800 °C. For preparing a structured photocatalytic reactor, a cylindrical quartz reactor (46 mm diameter, 200 mm length and 1 mm wall thickness), acting as pre-formed host channelling guide, was located within the reaction zone, whereas its outer surface was protected from the carbon nanotube growth by a sheet of graphite. In order to remove detrimental grease traces, the reactor was cleaned before synthesis by HCl acidic treatment followed by sonication in an ethanolic solution for 30 min. Generally, the growth duration was fixed at *ca.* 2–4 h depending on the needed final thickness of the aligned carbon nanotubes carpet.

2.2. Characterization techniques

X-ray diffraction (XRD) measurements were carried out on a D8-advance diffractometer equipped with a Vantec detector, in a $\theta/2\theta$ mode and using the $K\alpha_1$ radiation of Cu at 1.5406 Å.

The specific surface area measurements were performed on a ASAP2010 Micromeritics using N_2 as adsorbant at liquid N_2 temperature. Before the N_2 adsorption, the material was outgassed at 200 °C for 1 h in order to desorb the impurities or moisture from its surface. The surface areas were calculated by applying the B.E.T. and *t*-plot methods.

Scanning electron microscopy (SEM) was carried out on a Jeol JSM-6700F working at 3 kV voltage, equipped with a CCD camera. The sample was previously coated with gold and then deposited on a standard aluminum holder for observation.

The microstructure of the carbon nanotube was investigated by transmission electron microscopy (TEM) on a Topcon 002B microscope working with an accelerated voltage of 200 kV and a point-to-point resolution of 0.17 nm. The sample was sonically dispersed in an ethanol solution during 5 min and a drop of the solution was deposited onto a copper grid covered by a holey carbon membrane for observation.

The XPS measurements were performed at MULTILAB 2000 (TERMO) spectrometer equipped with Al Kα anode ($h\nu$ = 1486.6 eV). The C 1s peak at 284.2 eV was used to correct from charging effects. All the spectra were decomposed assuming several contributions, each of them having a Doniach–Sunjic shape and a Shirley background subtraction.

3. Results and discussion

3.1. Aligned carbon nanotube carpet

After the synthesis, the inner surface of the quartz tube was covered by a dense and homogeneous layer of aligned carbon nanotubes. The thickness of the carbon nanotube pattern could be accurately controlled by adjusting the synthesis duration, *i.e.* 1200 μm thickness for 2 h of synthesis and 250 μm for 0.5 h of synthesis. Fig. 1 shows SEM micrographs of the pattern of aligned carbon nanotubes grown on the quartz substrate for 0.5 h of synthesis. Low magnification images (Fig. 1A and B) clearly show the preferential orientation of the nanotubes perpendicularly with respect to the quartz substrate surface. The SEM observation also highlighted the extreme selectivity of the synthesis, since no nanoparticles were observed among the formed carbon products. High magnification SEM micrograph (Fig. 1C) indicates the relatively homogeneous diameter of the as-synthesized nanotubes with a high aspect ratio (length-to-diameter ratio). Representative high-resolution SEM micrograph (Fig. 1D) shows that the as-synthesized CNT have an average diameter of *ca.* 80 nm. Although the origin of the patterned growth mechanism was different and remained partly unclear up to now, similar results have already been reported by several groups [19,27,36]. It was noteworthy that the carbon nanotube array was relatively dense with a spacing of about 100 nm between neighbouring carbon nanotubes.

Careful SEM observation of the top of the carbon nanotube forest showed the absence of any iron particles attached at the tube tip. The observed results were in good agreement with those reported by Resasco during the growth of vertical single-walled carbon nanotube array on silica substrate, who described a root-growth mechanism in which the iron catalyst remained attached to the substrate surface and the nanotubes were slowly lift-off with aligned morphology [24]. The authors have also pointed out the significative influence of the catalyst concentration on the final morphology of the nanotubes, *i.e.* too low or too high catalyst

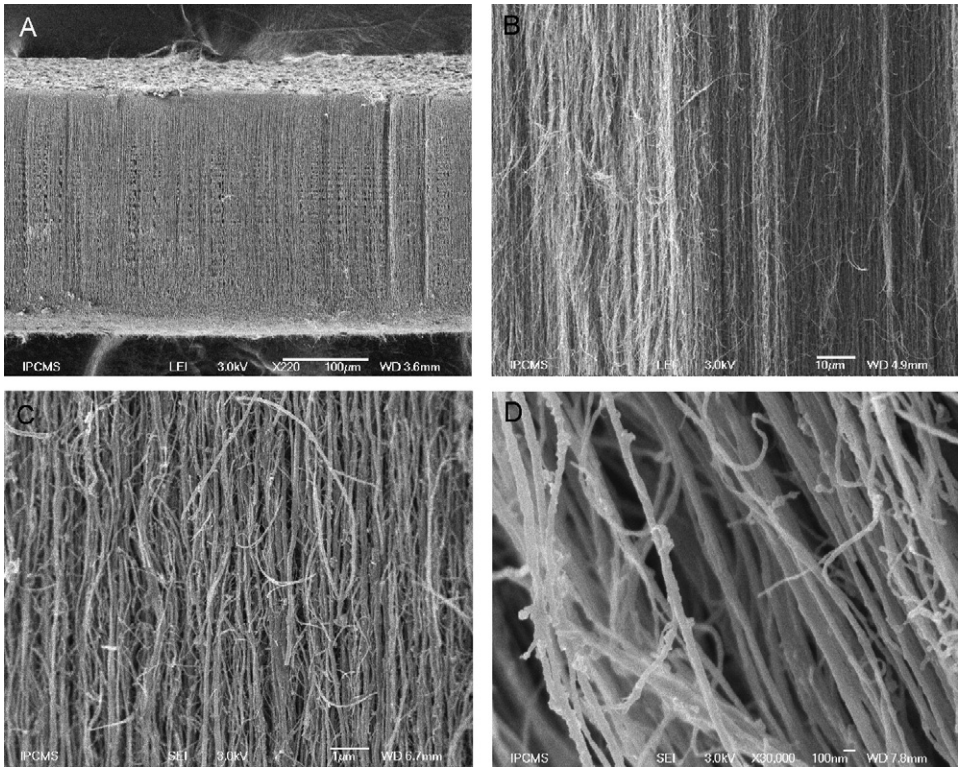

Fig. 1. SEM micrographs of the pattern of aligned carbon nanotubes grown on the quartz substrate after 30 min of synthesis. (A) Low magnification SEM micrograph showing the carbon nanotube carpet with thickness of *ca.* 250 μm. (B and C) Medium magnification SEM micrographs showing the regular structure of the aligned carbon nanotubes along the growth direction. (D) High magnification SEM micrograph of the carbon nanotubes in the carpet.

contents led to the formation of a 2D carbon nanotube disordered grass, whereas vertical nanotubes were perfectly grown with a medium catalyst amount.

The thickness of the carbon nanotube carpet could also be accurately controlled by adjusting the synthesis duration. Such a control was extremely advantageous especially in the case of the building of nanoporous filters for which the filter thickness could play an important role on the final performance of the device. Examples highlighting the thickness control are presented in Fig. 2. The diameter of the carbon nanotubes was hardly changed regardless the synthesis duration.

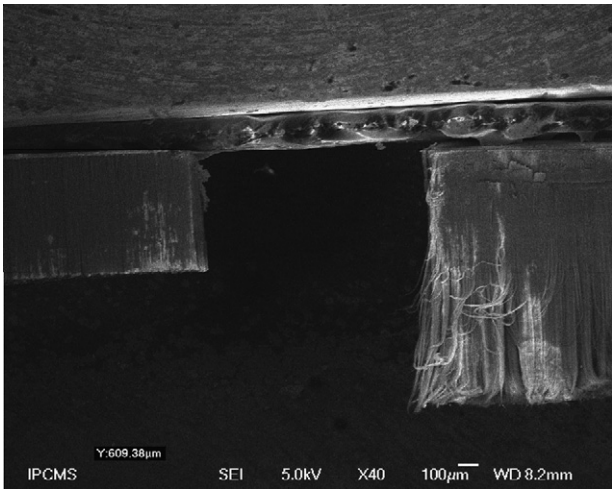

Fig. 2. SEM micrographs evidencing aligned carbon nanotube carpets with two different thicknesses obtained by tuning the reaction durations: (left) thickness of 600 μm, 1 h of synthesis; (right) thickness of 1200 μm, 3 h of synthesis.

The aligned carbon nanotube carpet was further treated in an acidic solution, HNO_3 30 vol.%, at 80 °C for overnight in order to remove from the sample the remaining iron-based catalyst. The sample was washed several times with distilled water until the pH reached a neutral value.

Low magnification TEM micrograph confirms the parallel orientation of the carbon nanotubes despite both grinding and sonication performed during the sample preparation for the TEM observation (Fig. 3A). TEM results also confirmed the homogeneous outer diameter of the formed carbon nanotubes, *ca.* 80 nm, with a length greater than several hundred micrometers leading to an aspect ratio greater than 5000. From high-resolution TEM image, one could also see that the tubes have open ends (Fig. 3B). It was noteworthy that the obtained tubes have a relatively narrow mean channel, *i.e.* 10 nm. TEM analysis also evidenced the absence of any iron catalyst particles on the outer surface of the tubes. Small-size iron particles were scarcely observed inside the tube channel, as already reported by Park and Keane [37] and by Anderson and Rodriguez [38]. This location resulted from the sucking of the starting iron catalyst inside the tube channel during its growth according to the results reported by Ermakova et al. [39]. High magnification TEM observation (not reported) shows that the residual iron-based catalyst was completely encapsulated under several graphene layers which render it inactive for the catalytic reaction.

High-resolution TEM observation also evidenced the low topological defect density compared to what is usually observed with tubes classically grown on supported catalysts [40]. An example of such a difference is presented in Fig. 4. This difference could be attributed to the higher synthesis temperature, *i.e.* 680 °C in the case of supported catalysts and 800 °C in the present work. It was expected that at a higher synthesis temperature, the pentagone (negative curvature) or heptagone (positive curvature)

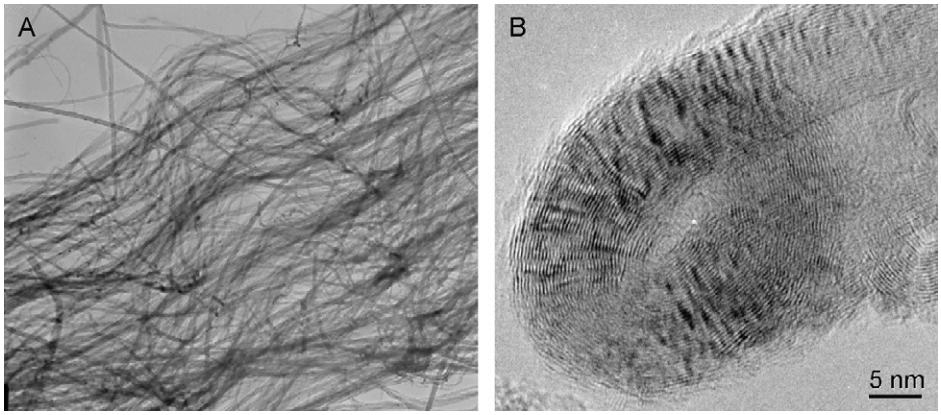

Fig. 3. Low (A) and high magnification (B) TEM micrographs of the aligned carbon nanotube network on quartz surface substrate.

insertion into the hexagone network was significantly lowered, thus, reducing the topoligical defects along the tube axis. The nature of the catalyst involved in the two synthesis processes, *i.e.* a homogeneous gas-phase feeding in the present work vs. solid anchored catalyst particles in the classical CCVD method, could also be responsible for such a difference.

The Raman spectrum recorded on the carbon nanotubes after acidic treatment exhibited a broad D band at 1342 cm^{-1} and the more intensive, narrower G band at 1608 cm^{-1}. These bands were attributed to the lattice defects, inducing a breaking of the 2D translational symmetry [41]. The D band is characteristic of sp^2 disordered carbon while the G band reflects the ordered carbon structure or in other words, the graphitization of the material.

The acidic treatment carried out in order to remove the residual iron catalyst from the carbon nanotube sample also introduced oxygenated functional groups at the tube surface, *i.e.* carboxylic acid, phenolic, acid anhydride, lactone or quinoic [42,43]. Indeed, all carbon forms are metastable against exposure to oxygen-containing gases or oxidizing agents such as nitric acid, sulfuric acid, etc. Introducing oxygen-containing groups at the carbon nanotube surface carbon – oxygenated function – significantly increased the solid interaction with polar molecules and rendered its more hydrophilic. The extent of hydrophilic interactions is closely linked to both density and chemical nature of the carbon–oxygenated functions. Such a hydrophilic character is expected to play an important role for the anchorage of foreign elements onto the carbon nanotube surface for subsequent catalytic applications.

The post-synthesis acidic treatment allowed the oxygen-to-carbon surface atomic ratio to be increased from a factor 10, in good agreement with the literature [44]. It was noteworthy that these oxygenated groups could be easily removed in a controlled way by heat treatment of the sample in flowing inert gas. Fig. 5A shows the oxygen-to-carbon surface atomic ratio determined by XPS as a function of the thermal treatment carried out on carbon nanotubes in flowing argon. The heat treatment allows one to control in a precise manner the location of the active phase with respect to the carbon nanotube surface depending on the downstream application. Indeed, on such heat treated material the deposition of the active phase via an aqueous solution only occurred inside the channel as aqueous liquid was steadily sucked inside the tube channel by capillarity forces while the hydrophobic character of the heat treated tube prevents any outer surface wetting. A controlled and exclusive deposition of iron oxide nanoparticles with respect to the carbon nanotube channel is presented in Fig. 5B. Work is on going to get more insight about the nature of the iron–carbon interface and the possible electronic interaction with the carbon nanotube inner wall.

The aligned carbon nanotube carpet was strongly anchored at the quartz substrate surface and almost no matter loss was observed after sonication of the sample in an ethanolic solution for 30 min. However, it is noteworthy that the carbon nanotubes array can also be grow on an amorphous silica, SiO_2, layer deposited on a host substrate. The strong anchorage of the carbon phase on the SiO_2 substrate surface was tentatively attributed to the penetration of the formed carbon nanotubes inside the SiO_2 matrix topmost layers of the macroscopic host structure. During the course of the synthesis, the fine and uniform droplets of $FeCp_2$ and C_7H_8 molecules fragment when entering into the high-temperature part of the reactor, leading to the formation of iron clusters along with C_x or CH_x species and hydrogen in the gas phase. Due to the high temperature, these clusters, Fe and C_x and CH_x, get sintering in a gas phase leading to the formation of fragments with larger size and further condensing on the quartz substrate with the concomitant formation of deposited nanoparticles playing a role of seed for the further growth process. Due to the relatively high reaction temperature, the metal nanoparticles strongly reacted with the quartz substrate or hydroxyl groups leading to an interface with high mechanical strength. The exposed metal (or solid solution between metal and dissolved carbon) further reacted with the surrounding C_x or CH_x species which initiated the first layer of carbon nanotubes. The continuous feeding of both metal and carbon species allowed the growth process to be maintained, leading to the formation of carbon nanotubes with increasing length. Due to the close location of the metal carpet at the beginning of the synthesis, the alignment could be imposed by steric hindrance leading to the final formation of well-aligned carbon nanotube array from the macroscopic host substrate. The carbon nanotubes with macroscopic shaping could be synthesized with different shapes, *i.e.* plate, cylinder, etc., and with different substrate sizes depending on the targeted downstream applications. The host structure could be also varied on a large range, *i.e.* quartz, stainless steel, graphite, etc., which significantly widens the range of applications and especially those involving aggressive media.

The specific surface area of the carbon nanotubes was ranged between 60 and 100 $m^2\ g^{-1}$, in line with that usually reported in the literature [41,45,46]. It was noteworthy that the surface area of the carbon nanotubes was mainly derived from the nanoscopic size of the material and not from a porosity network like in traditional supports.

Depending on the target application, self-supported carbon nanotube carpets could be obtained by dissolving the quartz host substrate in a HF solution. Examples of such nano–macro 1D carbon composites with different size and shape are presented in

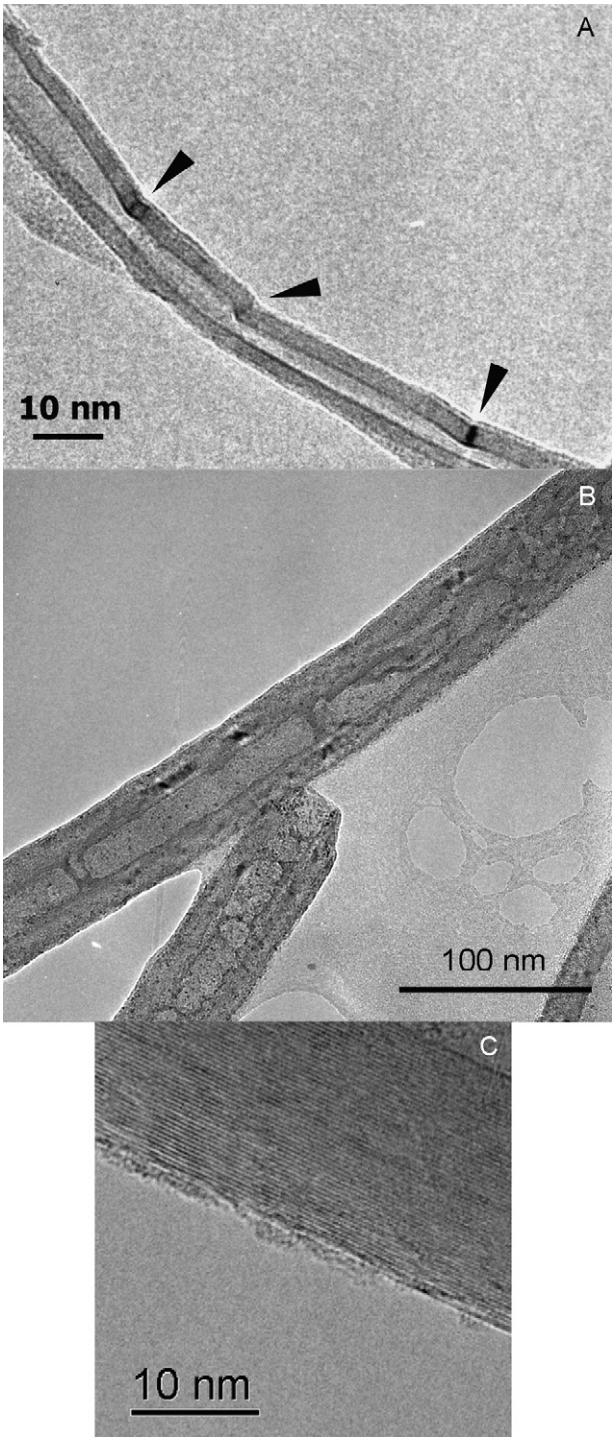

Fig. 4. TEM micrographs of the carbon nanotubes (A) synthesized by a classical CCVD method, *i.e.* on a fixed-bed supported catalyst, and (B and C) obtained in the presence of a mixture of ferrocene and toluene, *i.e.* gaseous catalyst. The low topological defect density and the high graphitisation were attributed to the relatively high synthesis temperature.

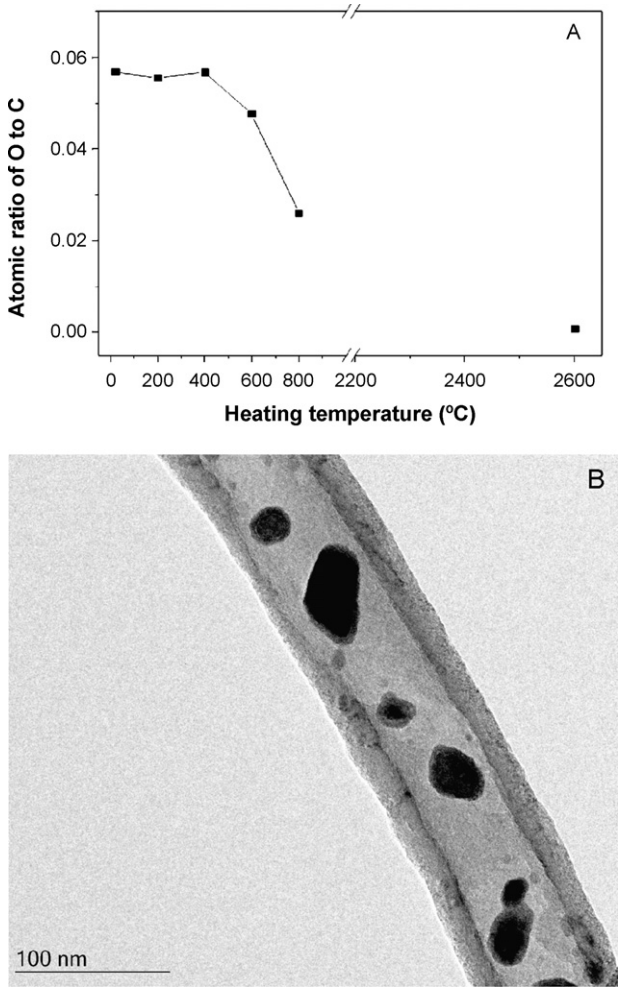

Fig. 5. (A) Surface atomic ratio of oxygen to carbon as a function of the treatment temperature determined by XPS semi-quantitative estimation using the usual Scofield coefficients. (B) Iron oxide nanoparticles exclusively located inside the carbon nanotube channel after heat treatment at high temperature to remove the oxygenated functional groups from the surface.

Fig. 6. The macronized nanotube structure obtained was found to have a very high mechanical strength and could be handled easily without damage. Sonication of the macronized nanotubes in an ethanolic solution for hours resulted in no matter loss, indicating the high mechanical stability of the nanotube assembly. The high mechanical strength observed could result from the wetting and drying processes performed for cleaning the nanotubes after synthesis, either during the post-synthesis acid treatment or during the rinsing with water. Wetting and drying would induce the tube gathering by the van der Waals forces. Indeed, removal of water during the drying process causes the inter-tube distance to decrease by the action of liquid bridging [47,48]. The evidence of the action of capillarity forces induced by water was provided by the compaction of bucky paper that occured after the drying process of filtered bucky paper. The removal of the water inside the material can induce a strong isotropic contraction of the block due to the decrease of the inter-tube distance as a function of water evaporation. The same phenomenon could be also obtained by replacing water by other solvents, *i.e.* sulfuric acid [49]. When a plane quartz host substrate was used, it was noteworthy that the final self-supported aligned carbon nanotube sheet remained relatively plane after drying, indicating the almost absence of moisture gradient throughout the sample thickness (Fig. 6B). This allows the final macrostructure to be totally designed by targeting the geometry of the host substrate.

3.2. Liquid-phase hydrogenation

Selective hydrogenation of organic compounds is a crucial process in the manufacture of petrochemicals and fine chemicals. The metals generally used as catalyst in such reactions are

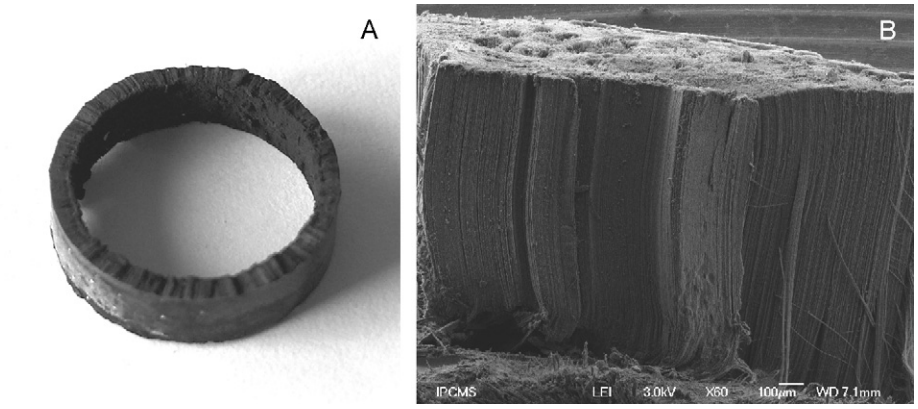

Fig. 6. Macrostructures of self-supported aligned carbon nanotubes obtained after dissolving the quartz growth substrate in a HF solution: (A) ring and (B) plate.

palladium and platinum, pure or doped with foreign elements, supported on high specific surface area activated charcoal. The hydrogenation of cinnamaldehyde is a parallel and consecutive reduction of different functional groups in the same starting substrate, *i.e.* C=C and C=O hydrogenation leading to the formation of the hydrocinnamaldehyde and the unsaturated alcohol, respectively [50–52]. The hydrogenation activity obtained on the aligned carbon nanotubes supported palladium (5 wt.%)/aligned CNTs catalyst as a function of the experiment time is presented in Fig. 7A. The carbon nanotubes were directly grown on the interior surface of a cylindrical quartz reactor (Fig. 7B) which was subsequently employed as stirrer and thus, no catalyst deterioration occurred during the course of the reaction. For comparison, the hydrogenation activity of the Pd supported on fluffy carbon nanotubes was also reported in the same figure (Fig. 7A). The fluffy CNT supported Pd catalyst exhibits a higher hydrogenation activity compared to that observed on the aligned CNT-based catalyst. Such a difference in terms of hydrogenation activity was attributed to the higher facility of liquid products to access to the metal particles located on the outer surface of the nanotubes. In the case of aligned carbon nanotubes, the relatively small inter-tube distance make the liquid circulation more difficult and thus, leading to a lower reactivity under similar reaction conditions. It is noteworthy that the density of the carbon nanotubes array can be partly controlled by adjusting the catalyst concentration. Such work is on going with the aim of building new nanoscopic system with lower resistance to liquid diffusion. However, this result showed a first step towards an efficient and realistic use of CNTs for liquid-phase applications, by means of stable non-fluffy CNTs with macroscopic shape control.

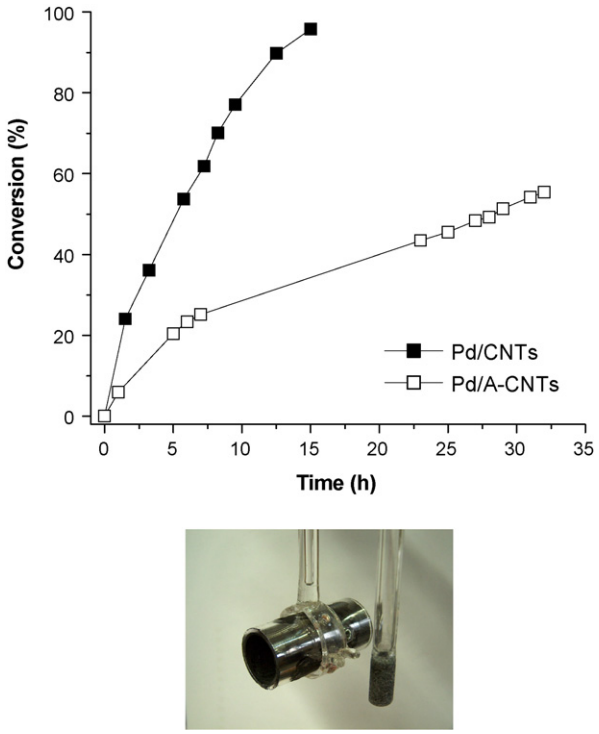

Fig. 7. (Top) Liquid-phase hydrogenation of cinnamaldehyde on the Pd (5 wt.%)/aligned carbon nanotube (□: Pd/A-CNTs) and Pd (5 wt.%)/bulk CNT (■: Pd/CNTs) catalysts at 80 °C in a batch mode. Reaction conditions: 25 mL of cinnamaldehyde in 500 mL of dioxane solvent, H_2 flow rate = 50 mL min^{-1}, stirring rate = 250 rpm, atmospheric pressure. (Down) Optical micrograph of the quartz reactor holding aligned CNT in the inner surface.

According to previous results obtained on palladium decorating carbon nanotubes, the C=C bond hydrogenation was the fastest reaction, leading to the formation of hydrocinnamaldehyde. The main secondary reaction, *i.e.* the total hydrogenation to cinnamylalcohol, also occurred but was several times slower, leading to an extremely high selectivity to hydrocinnamaldehyde of >90%. Apparently, the adsorption occurs on the palladium surface mainly through the C=C bond, in good agreement with the literature results [53].

Similar results have also been reported in the case of bulk carbon nanofibers and nanotubes with random orientation [54–56]. Although they clearly pointed out the clear superiority of the fluffy non-aligned carbon nanotube versus the high surface area activated charcoal catalyst in terms of selectivity, the use of such bulk nanomaterial catalysts remained prohibited by the tedious catalyst recovery step, due to the nanoscopic size of the support which requires a high performance filtration. In the present case, the extremely easy catalyst–product separation, due to the macroscopic shape of the nanodesigned catalyst, thus led to phase-out the post-reaction filtration step which is a time/energy consuming and waste generating step.

3.3. Ceramic nanoporous membrane

Fibrous filters are the most common type of filter media and are usually made from cellulose, glass, or polymer fibers. All these filters suffer from a low mechanical resistance and a low oxidative resistance to allow them to work at high temperature or under harsh conditions. The problem linked to the filter regeneration also calls for the development of a new type of filters with higher performances. The fibrous aerosol filter efficiency is titeny

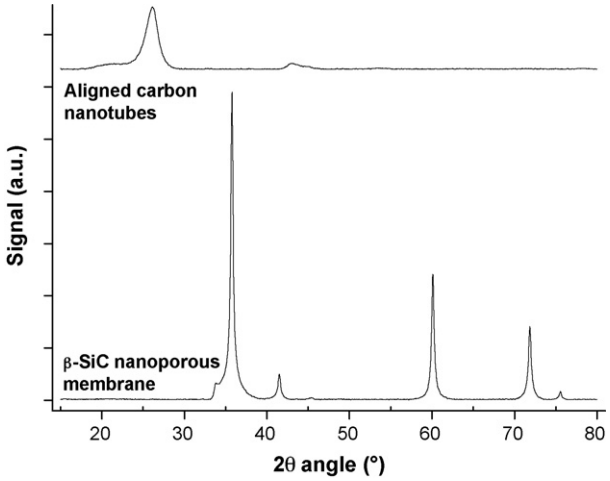

Fig. 8. XRD patterns of the aligned carbon nanotube carpet and of the self-supported nanoporous β-SiC material.

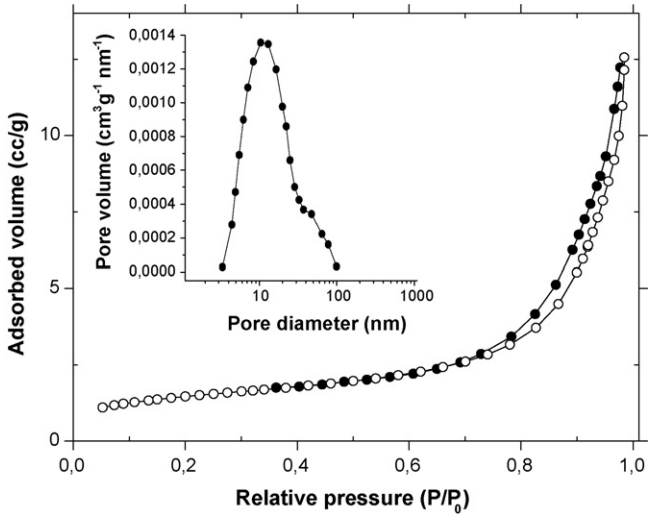

Fig. 10. Nitrogen adsorption–desorption isotherms and pore size distribution of the β-SiC ceramic nanoporous material.

depending on the fiber surface, the inertial impaction of a particle on a fiber, and the Brownian diffusion of particles in the filter pores. It is expected that filters with smaller size fibers could exhibit higher filtration performance compared to the traditional ones. Since carbon filters are still suffer for progressive oxidative degradation, it is thus of interest to develop a new generation of filters with higher stability, *i.e.* ceramic nanoporous filters.

For this specific application, the aligned carbon nanotube carpet could be seen as a morphological template precursor for synthesizing nanoporous SiC with a controlled and structured nanoporosity. Before infiltration the carbon nanotubes carpet was treated in an aqua regia solution for overnight at 80 °C in order to remove as much as possible the residual iron catalyst inside the solid matrix. ATG analysis on the acidic treated sample indicates that the residual iron-based compounds inside the sample after acidic treatment was *ca.* 0.2 wt.%. This iron phase was attributed to the iron nanoparticles encapsulated by graphene layers inside the tube channel. The synthesis process was to infiltrate the carbon nanotube carpet with a polymer ceramic leading to the formation of a nanoporous ceramic membrane after a subsequent heat treatment and calcination in order to remove the nanocarbon template. The final SiC membrane was treated with an acidic solution in order to remove the residual iron-based compounds inside the channel. The process used the known chemical inertness of bulk SiC towards oxidation to perform the selective removal of the aligned nanocarbon template. Nanoporous SiC with macroscopic shaping was synthesized by infiltration of the aligned carbon nanotube carpet with a solution of allylhydridopolycarbosilane (AHPCS, SMP-10, Starfire Systems, Inc.), with a viscosity of 45–120 cP and a density of 0.998 g cm^{-3}. The SMP-10 polymeric solution, acting as SiC precursor, was diluted in tetrahydrofurane (THF, Aldrich) to yield solution with a concentration of 25 wt.%. A piece of aligned carbon nanotubes anchored on a quartz substrate (4 cm × 4 cm) was fixed on a spin coater holder and further infiltrated by of SMP-10/THF solution. The infiltrated composite was dried and cured at 180 °C for 24 h under vacuum, before to undergo a second and similar infiltration cycle in order to ensure the complete filling of the inter-tube space, taking into account a yield to SiC of 80% from the starting polymer precursor after thermal treatment at 1000 °C (data from Starfire Syst. Inc.). The cured sample was further carburized in flowing nitrogen at 1000 °C for 2 h (heating rate of 1 °C min^{-1}). The carburized composite was subsequently calcined in air at 700 °C for 1 h in order to remove the remaining unreacted carbon nanotubes. The removal of non-transformed aligned carbon nanotubes by burning was the key-step of the process, since it created a one dimensional anisotropic nanoporous network with a mean diameter of *ca.* 40–60 nm. Fig. 8 shows the XRD patterns of the aligned carbon nanotube carpet precursor and of the nanoporous β-SiC material obtained after the nanotube carpet template removal. Before the SiC formation, the low intensity diffraction peaks corresponding to the carbon nanotube carpet was observed. By contrast, the XRD pattern of

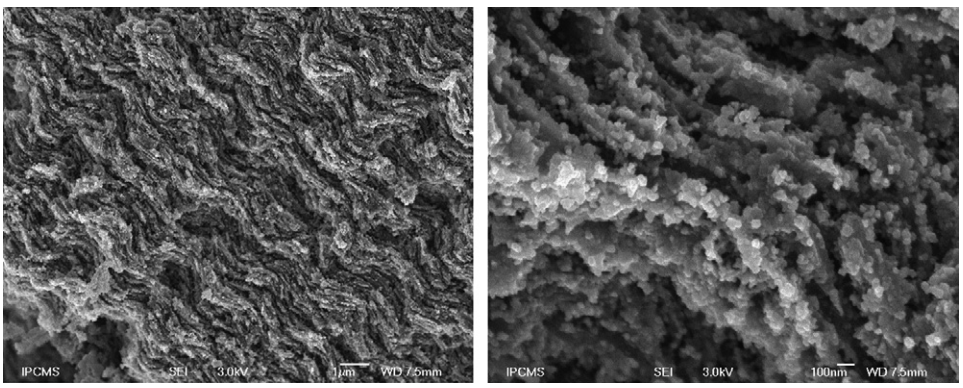

Fig. 9. SEM micrographs with different magnifications of the SiC ceramic nanoporous filter after air calcination to remove the aligned carbon nanotube carpet template. The void channels could be considered as a negative replica of the carbon nanotube morphology.

the resulting nanoporous SiC material only showed the diffraction lines corresponding to β-SiC in the fcc structure, no traces of other compounds such as residual carbon, SiO_2 or Si were detected, meaning that such species if present were either in very small crystalline amounts or in a superficial amorphous form, not accurately detected by XRD.

Finally, the quartz substrate was dissolved in a HF solution at room temperature and the self-supported SiC nanoporous material was obtained. The void channels could be considered as a negative replica of the carbon nanotube morphology. The SEM micrographs of Fig. 9 evidenced the 1D nanoporous network of such a SiC ceramic nanomembrane, resulting directly from the burning of the remaining unreacted aligned carbon nanotubes. Fig. 10 shows the nitrogen adsorption–desorption isotherm and the pore size distribution of the β-SiC nanoporous material, evidencing the creation of a new porosity. The material had a specific surface area of 117 $m^2\ g^{-1}$ with no microporosity and a pore size distribution centered around 10–20 nm and ranging up to about 100 nm. This was in agreement with the generation of surface area and porosity by channels resulting from the oxidation of the carbon nanotube template, with mean diameter in the 40–60 nm range. Work is on going to get more insight about the relationship between the average diameter of the aligned carbon nanotube precursor and the mean pore size of the created nanochannels, since (i) part of the carbon nanotube walls could react with SMP-10 to form the carbide leading to mean nanochannel with bigger diameter than the starting carbon nanotube and (ii) some slight sintering could occur, leading to close some small size channels and to enlarge other ones.

4. Conclusion

In summary, aligned carbon nanotubes with various macroscopic shapes could be efficiently synthesized through a CCVD process with a mixture of ferrocene and toluene at mild temperature, *ca.* 800 °C. The strong anchorage of the carbon nanomaterial at the macroscopic host surface allows the nano–macro-composite to be efficiently used as catalyst support for several reactions. The carbon nanotube carpet thickness could be accurately controlled from few tenth micrometers to more than few millimeters by tuning the synthesis duration, depending on the requirements to meet in downstream applications. In addition, the surface hydrophilicity–hydrophobicity could be also precisely tuned by submitting the sample either to an acidic or thermal treatment. The acidic treatment introduced oxygenated functional groups at the carbon surface and thus increased the hydrophilicity, whereas the thermal treatment turned it to a more hydrophobic character.

The carbon nanotube array could be efficiently used as removable precursor template in the design of β-SiC ceramic nanoporous membranes, for applications in the filtration field under harsh conditions. The fine control of the filter channel renders it promising for use in the filtration of fine particulate matter such as viruses from water or in airborne conditions. Work is on going on such highly challenging fields and will be presented in the near future.

Acknowledgements

The at SiC company is thanked for supporting part of the study. The authors would like to acknowledge Alain Carvalho (IPCMS, UMR 7504 CNRS) for help during the synthesis of the aligned carbon nanotubes on the quartz substrate. Pierre Bernhardt and Dr. Thierry Dintzer (LMSPC) are gratefully acknowledged for performing XPS and SEM, respectively. Dr. Ovidiu Ersen (IPCMS) is deeply thanked for performing TEM experiments and for helpful discussion during the preparation of the manuscript. TEM and SEM experiments were carried out at the facilities of the IPCMS.

References

[1] S. Iijima, Nature (London) 354 (1991) 56.
[2] P.M. Ajayan, Chem. Rev. (1999) 1797.
[3] K.P. de Jong, J.W. Geus, Catal. Rev. -Sci. Eng. 42 (4) (2000) 481.
[4] R. Andrews, D. Jacques, D. Qian, T. Randell, Acc. Chem. Res. 35 (2002) 1008.
[5] Ph. Serp, M. Corrias, Ph. Kalck, Appl. Catal. A: Gen. 253 (2003) 337.
[6] M.J. Ledoux, C. Pham-Huu, Catal. Today 102–103 (2005) 2.
[7] J.M. Bonard, L. Forro, D. Ugarte, W.A. De Herr, A. Châtelain, Eur. Chem. Chron. 3 (1998) 9–16.
[8] C. Emmenegger, J.M. Bonard, P. Mauron, P. Sudan, A. Lepora, B. Grobet, A. Züttel, L. Schlapbach, Carbon 41 (2003) 539.
[9] S. Tang, Z. Zhong, Z. Xiong, L. Sun, L. Liu, J. Lin, Z.X. Shen, K.L. Tan, Phys. Lett. 350 (2001) 19.
[10] H. Dai, Topics in Applied Physics, Nanotube Growth and Characterization, vol. 80, Springer-Verlag, Berlin/Heidelberg, 2001, p. 32.
[11] Z. Pan, H. Zhu, Z. Zhang, H-j. Im, S. Dai, D.B. Beach, D.H. Lowndes, J. Phys. Chem. B 107 (2003) 1338.
[12] C. Pham-Huu, R. Vieira, M. J. Ledoux, L. Charbonnière, R. Ziessel, French Pat. Appl. No. 01 15178, assigned to Sicat SA (2001).
[13] M.J. Ledoux, R. Vieira, C. Pham-Huu, N. Keller, J. Catal. 216 (1–2) (2003) 333.
[14] R. Vieira, M.J. Ledoux, C. Pham-Huu, Appl. Catal. A 274 (2004) 1.
[15] P. Li, T. Li, J.-H. Zhou, Z.-J. Sui, Y.-C. Dai, W.-K. Yuan, De Chen, Micr. Mesopor. Mater. 95 (1–3) (2006) 1.
[16] N.A. Jarrah, J.G. van Ommen, L. Lefferts, J. Catal. 239 (2) (2006) 460.
[17] M.K. van der Lee, A.J. van Dillen, J.W. Geus, K.P. de Jong, J.H. Bitter, Carbon 44 (4) (2006) 629.
[18] K. Hata, D.N. Futaba, K. Mizuno, T. Namai, M. Yumura, S. Iijima, Science (2004) 19.
[19] X. Li, A. Cao, Y.J. Jung, R. Vajtai, P.M. Ajayan, Nano Lett. 5 (10) (2005) 1997.
[20] M. Pinault, V. Pichot, H. Khodja, P. Launois, C. Reynaud, M. Mayne-L'Hermitte, Nano Lett. 5 (12) (2005) 2394.
[21] L. Zhu, Y. Xiu, D.W. Hess, C.P. Wong, Nano Lett. 5 (12) (2005) 2641.
[22] M. Hu, Y. Murakami, M. Ogura, S. Maruyama, T. Okubo, J. Catal. 225 (2004) 230.
[23] S. Maruyama, E. Einarsson, Y. Murakami, T. Edamura, Chem. Phys. Lett. 403 (2005) 320.
[24] L. Zhang, Y. Tan, D.E. Resasco, Chem. Phys. Lett. 422 (2006) 198.
[25] I. Janowska, G. Winé, M.J. Ledoux, C. Pham-Huu, J. Mol. Catal. A: Chem. 267 (2007) 92.
[26] G. Viswanathan, D.B. Kane, P.J. Lipowicz, Adv. Mater. 16 (2004) 2045.
[27] A. Srivastava, O.N. Srivastava, S. Talapatra, R. Vajtai, P.M. Ajayan, Nature Mater. 3 (2004) 610.
[28] L. Zhu, Y. Sun, D.W. Hess, Ch.P. Wong, Nano Lett. 6 (2) (2006) 243.
[29] H. Peng, J. Am. Chem. Soc. 130 (2008) 42.
[30] J.M. Nhut, R. Vieira, L. Pesant, J.P. Tessonnier, N. Keller, G. Ehret, C. Pham-Huu, M.J. Ledoux, Catal. Today 76 (2002) 11.
[31] J.M. Nhut, L. Pesant, J.P. Tessonnier, G. Winé, J. Guille, C. Pham-Huu, M.J. Ledoux, Appl. Catal. A: Gen. 254 (2003) 345.
[32] J.M. Nhut, N. Keller, P. Nguyen, C. Pham-Huu, M.J. Ledoux, Catal. Today 92 (2004) 91.
[33] B.J. Hinds, N. Chopra, T. Rantell, R. Andrews, V. Gavalas, L.G. Bachas, Science 303 (2004) 62.
[34] M.J. Casavant, D.A. Walters, J.J. Schmidt, R.E. Smalley, J. Appl. Phys. 93 (2003) 2153.
[35] S.A. Miller, V.Y. Young, C.R. Martin, J. Am. Chem. Soc. 123 (2001) 12335.
[36] A.L. Elias, J.A. Rodriguez-Manzo, M.R. McCartney, D. Golberg, A. Zamudio, S.E. Baltazar, F. Lopez-Urias, E. Munoz-Sandoval, L. Gu, C.C. Tang, D.J. Smith, Y. Bando, H. Terrones, M. Terrones, Nano Lett. 5 (2005) 467.
[37] C. Park, M.A. Keane, Langmuir 17 (2001) 8386.
[38] P.E. Anderson, N.M. Rodriguez, Chem. Mater. 12 (2000) 823.
[39] M.A. Ermakova, D.Y. Ermakov, A.L. Chuvilin, G.G. Kuvshinov, J. Catal. 201 (2001) 183.
[40] (a) N. Zhao, C. He, J. Li, Z. Jiang, Y. Li, Mater. Res. Bull. 41 (2006) 2204;
(b) Q.-M. Gong, Z. Li, Y. Wang, B. Wu, Z. Zhang, J. Liang, Mater. Res. Bull. 42 (2007) 474.
[41] Ch.-M. Chen, Y.-M. Dai, J.G. Huang, J.-M. Jehng, Carbon 44 (2006) 1808.
[42] A. Kuznetsova, I. Popova, J.T. Yates, M.J. Bronikowski, C.B. Huffman, J. Liu, R.E. Smalley, H.H. Hwu, J.G. Chen, J. Am. Chem. Soc. 123 (2001) 10699.
[43] T. Kyotani, S. Nakazaki, W.-H. Xu, A. Tomita, Carbon 39 (2001) 782.
[44] T.G. Ros, A.J. van Dillen, J.W. Geus, D.C. Koningsberger, Chem. Eur. J. 8 (5) (2002) 1151.
[45] G. Gulino, R. Vieira, J. Amadou, P. Nguyen, M.J. Ledoux, S. Galvagno, G. Centi, C. Pham-Huu, Appl. Catal. A: Gen. 279 (2005) 89.
[46] A. Peigney, Ch. Laurent, E. Flahaut, R.R. Bacsa, A. Rousset, Carbon 39 (2001) 507.
[47] X. Rondeau, C. Affolter, L. Komunjer, D. Clausse, P. Guigon, Powder Technol. 130 (2003) 124.
[48] P.G. Whitten, G.M. Spinks, G.G. Wallace, Carbon 43 (2005) 1891.
[49] L.M. Ericson, H. Fan, H. Peng, V.A. Davis, W. Zhou, J. Sulpizio, Y. Wang, R. Booker, J. Vavro, C. Guthy, A.N.G. Parra-Vasquez, M.J. Kim, S. Ramesh, R.K. Saini, C. Kittrell, G.

Lavin, H. Schmidt, W.W. Adams, W.E. Billups, M. Pasquali, W.F. Hwang, R.H. Hauge, J.E. Fischer, R.E. Smalley, Science 305 (2004) 1447.
[50] P. Kluson, L. Cerveny, Appl. Catal. A 128 (1995) 13.
[51] V. Ponec, Appl. Catal. A 149 (1997) 27.
[52] B. Coq, F. Figueras, Coord. Chem. Rev. 178–180 (1998) 1753.
[53] P.N. Rylander, Catalytic Hydrogenation in Organic Synthesis, Academic Press, New York, 1979, p. 72.
[54] J.P. Tessonnier, L. Pesant, C. Pham-Huu, G. Ehret, M.J. Ledoux, Stud. Surf. Sci. Catal. 143 (2002) 697.
[55] C. Pham-Huu, N. Keller, L.J. Charbonnière, R. Ziessel, M.J. Ledoux, Chem. Commun. (2000) 1871.
[56] C. Pham-Huu, N. Keller, G. Ehret, L. Charbonnière, R. Ziessel, M.-J. Ledoux, J. Mol. Catal. A: Chem. 170 (2001) 155.